J. Fluid Mech. (1988), *vol.* 187, *pp.* 573–588
Printed in Great Britain

Pressure drop and power dissipation in oscillatory wavy-walled-tube flows

By M. E. RALPH
Smith Associates Ltd, Surrey Research Park, Guildford, Surrey GU2 5YP, UK

(Received 5 September 1986 and in revised form 3 April 1987)

Pressure drops occurring in oscillatory viscous flows in wavy-walled tubes have been studied experimentally, for Reynolds numbers up to 1500 and Strouhal numbers in the range 0.005 to 0.02, and by numerical solution of the Navier–Stokes equations, for Reynolds numbers up to 200 and Strouhal numbers between 0.005 and 0.1. Agreement was good for values of the mean modulus of the pressure drop at lower Strouhal numbers and for values of the mean power dissipation at all Strouhal numbers.

Numerical solutions have shown that the pressure drop may vary non-sinusoidally, even though the imposed variation in flow rate is sinusoidal. This cannot be explained by the nonlinearity of the steady pressure drop–flow rate relationship, and arises because the velocity field is not quasi-steady. In particular energy may be stored in strong vortices formed during the acceleration phase of the flow cycle, and partially returned to the main flow later. The peak pressure drops in such flows, which are associated with the formation of these vortices, can be almost twice as large as values predicted by adding the appropriate quasi-steady and unsteady inertial contributions. This finding is important in the wider context of unsteady conduit flow.

The dependences of the mean modulus of the pressure drop and the mean power dissipation on the Strouhal number and frequency parameter were investigated in detail numerically for two geometries. It was not possible to reduce either dependence to a function of a single parameter. The 'equivalent' straight-walled tube for power dissipation was found to have a smaller bore than that for pressure drop, leading to smaller 'phase angles' than might have been expected at large values of the frequency parameter. This is because as the pressure drop becomes increasingly dominated by unsteady inertia, there remain relatively large recirculations in which energy is dissipated.

1. Introduction

In membrane oxygenators, the resistance to gas transfer is due primarily to the resistance of the mass transfer boundary layer within the blood, rather than that of the membrane itself (Chang & Mockros 1971). This has meant that transfer rates have been enhanced significantly by inducing stirring motions in the flowing blood, and a successful design has been that of Bellhouse *et al.* (1973), utilizing pulsatile flows across furrowed membranes. The fluid mechanics of these devices has been the subject of a number of studies (Bellhouse & Snuggs 1977; Sobey 1980 and

Stephanoff, Sobey & Bellhouse 1980). Similar flow patterns can occur in wavy-walled tubes (Ralph 1985, 1986), which are therefore likely to offer an alternative geometry to the furrowed channel. An important advantage of the axisymmetric design is that the blood conduits can be self-supporting, instead of requiring moulded backing plates, which are expensive to construct. One purpose of the present work is to supplement published details of wavy-walled-tube flow patterns with data on the unsteady pressure drops. The wider industrial importance of periodic flows in conjunction with non-uniform walls has recently been emphasized by Ghaddar *et al.* (1986).

Numerical studies of related unsteady flows, in which solutions to the Navier–Stokes equations have been obtained by finite differences, have included those of Cheng, Clark & Robertson (1972) and Cheng, Robertson & Clark (1973), who studied flows near square occlusions in planar channels. Daly (1976) considered smooth axisymmetric stenoses, and Savvides & Gerrard (1984) predicted pressure drops in tubes with triangular corrugations of relatively small amplitude, representing arterial prostheses.

The present work differs from those just cited in that results have been obtained both by experimental measurements and by finite-difference solution of the governing equations, giving greater confidence in accuracy where the agreement is good. In addition, a wider range of flow parameters is covered than previously, and an attempt has been made to understand in detail the underlying physical processes. The content of the paper is as follows. The formulation of the problem and the method of calculation of the pressure drop are given briefly in §2, where the experimental methods are also described. In §3, the variations of the pressure drop with time in typical flows are discussed, whilst in §4 the variation of the mean modulus of the pressure drop is given as a function of the governing parameters. §5 deals with power dissipation and the phase relationship between the pressure drop and the flow rate, and conclusions are offered in §6.

2. Numerical and experimental methods

2.1. *Formulation and computation of pressure drop*

The formulation of the problem and numerical methods of solution are given elsewhere (Ralph 1985, 1986). Only the relevant definitions are repeated here, and the method of computing the pressure drop described. The flow is governed by a Strouhal number St and a frequency parameter α^2 defined by

$$St = \frac{\hat{a}\hat{f}}{\hat{U}_0} \tag{1}$$

and

$$\alpha^2 = \frac{\hat{a}^2\hat{f}}{\hat{\nu}}, \tag{2}$$

where $\hat{a}$ is the radius of the tube at the cross-section of smallest area, $\hat{f}$ is the frequency of the time-variation in flow rate, $\hat{\nu}$ is the kinematic viscosity and $\hat{U}_0$ is a reference velocity. (Note that dimensional quantities are denoted throughout by carets.) $\hat{U}_0$ is given by

$$\hat{U}_0 = \frac{\hat{Q}_0}{\pi\hat{a}^2}, \tag{3}$$

where $\hat{Q}_0$ is the maximum volumetric flow. The flow rate Q is sinusoidally varying with zero mean, so that

$$\hat{Q} = \hat{Q}_0 \sin 2\pi \hat{f}\hat{t}, \tag{4}$$

where $\hat{t}$ is the dimensional time. The dimensionless time t is defined as $\hat{t}\hat{f}$. We note that the ratio $\alpha^2/St = \hat{U}_0 \hat{a}/\hat{\nu}$, represents the Reynolds number at peak flow, and will be denoted by Re_0. The tube wall is axially periodic in shape, and is specified by the equation for the radius over a single wavelength:

$$\hat{r}_w = \hat{a}\left\{1 + \frac{D}{2}\left(1 - \cos\frac{2\pi\hat{x}}{\hat{a}L}\right)\right\}, \tag{5}$$

where $\hat{x}$ is the axial coordinate and $\hat{r}_w(\hat{x})$ the local tube radius. D and L are dimensionless geometrical parameters which take the values $L = 10$ and $D = 2$ throughout.

The pressure $\hat{p}$ is made dimensionless according to $\hat{p} = p\hat{\rho}\hat{U}_0^2$, where $\hat{\rho}$ is the fluid density. The axial pressure gradient can be expressed in terms of the vorticity field, and a finite-difference form of this expression was integrated numerically (using Simpson's rule) to obtain the pressure drop Δp_L between points on the wall separated by an axial distance $\hat{a}L$. The flow, and hence also the radial pressure gradient, are assumed to be axially periodic with wavelength $\hat{a}L$, and thus Δp_L represents the unique pressure drop per wall wavelength for all radial positions.

2.2. *Experimental method*

A wavy-walled tube was constructed in two pieces, each formed by pressing a stainless-steel mould, with a minimum diameter of 2 mm, into heat softened Perspex blocks. In order to guarantee uniformity of the cross-sections of minimum area, the diameter of the constrictions was enlarged by 0.1 mm, using a long drill of 2.1 mm diameter, and hence the wall shape was not precisely sinusoidal, but contained very short straight sections at the constrictions. The dimensionless geometric parameters were $L = 10$ and $D = 2$ (to within about 5%). The overall length of the model was 230 mm, with thirteen complete wavelengths and a 50 mm section of uniform 2.1 mm bore pipe at each end. Pressure tappings of 0.5 mm bore were drilled at the points of greatest cross-sectional area of the 2nd, 5th, 7th, 9th and 12th wavelengths.

Solutions of glycerol at concentrations in the range 0–78% by weight were used for the working fluid, and dynamic viscosities in the approximate range 1–50 cP were thereby obtained. Viscosity was measured using a rotary viscometer (Brookfield Synchro-Lectric LVT model with UL adapter), and repeat measurements were made frequently during a series of experiments. Comparison of measured viscosities with tabulated values, under standard conditions, showed the measurements to be accurate to within about 3%.

Oscillatory flows at frequencies between 2 and 10 Hz were produced using an adjustable-stroke Scotch-yoke mechanism driven by an electric motor (both a Parvalux 125 W shunt motor and an Eberhard-Bauer 115 W induction motor were used). The modified plunger and barrel of a 'Hamilton' gas chromatography syringe of 1 ml total volume (Perkin–Elmer) were used as a piston and cylinder to drive the flow, because of their excellent sealing properties and the small, accurately graduated volume of the barrel. Rigid piping connected the piston to the test section, whose other end was connected to a reservoir vented to the atmosphere. Flow contractions were incorporated at both ends of the test section. Instantaneous pressure differences were

measured by means of a piezoelectric differential pressure transducer (Kistler type 500). The output voltage was recorded using an Arrow LSI-11 computer with ADC-11 analogue-to-digital converter (ADC) and PRTC-11 programmable real-time clock. The linearity of the transducer and charge amplifier was calibrated against variable static heads of water and mercury, and dynamically calibrated in measurements of pressure drops in oscillating straight-walled tube flows. The range of peak-to-peak pressure differences to be measured was about 2 to 50 cm of water, and the charge amplifier sensitivity was adjusted so that peak-to-peak voltages were always about 10 V. The resolution of the ADC was about 5 mV.

The pressure tappings at the 2nd and 12th hollows were used throughout. Entrance effects had been shown to be negligible when these tappings were used in steady-flow experiments, provided the flow remained laminar (Ralph 1987), this is also expected to be true in oscillatory-flow experiments. Pressure tappings were connected to the transducer by short lengths of small-bore PVC tubing in which pressure waves would be expected to propagate at a finite rate. However, the estimated propagation times were much smaller than the imposed periods of oscillation and, in experiments in which the lengths of the connections were increased by factors of 2 and 3, no measurable effects on the phase angle between pressure drop and flow resulted.

Frequency was measured, to an accuracy of 1 ms, using a magnet mounted on the Scotch-yoke flywheel and a Hall-effect switch attached to the baseplate. The magnet also provided a reference phase position for the calculation of power dissipation. 200 pressure difference samples were taken during each cycle of oscillation, and samples were taken from two complete consecutive cycles in order to eliminate the effect of transducer 'drift'. The resulting data values were converted to dimensionless form and used to compute certain global measures of the pressure drop.

3. Numerical predictions of the variation of the pressure drop with time

In figure 1, the computed dimensionless pressure drop Δp_L is shown as a function of time for four pairs of values of Re_0 and St. It is striking that all the figures show departures from sinusoidal form, even though the flow rate varies sinusoidally. Specifically, in figure 1 (*a*) there are marked points of inflexion where the magnitude of the pressure drop is increasing, near the times $t = 0.1$ and $t = 0.6$; in figure 1 (*b*) these inflexion points have become subsidiary turning points and there are strong additional points of inflexion near the times $t = 0.35$ and $t = 0.85$; in figure 1 (*c*) there are points of inflexion where the magnitude of the pressure drop is decreasing; and in figure 1 (*d*) there is a marked inflexion point at $t \approx 0.15$, but no corresponding feature in the second half of the flow cycle. The Strouhal-number range represented in these figures is 0.01 to 0.035, which corresponds approximately to that utilized in the oxygenators of Bellhouse *et al.* (1973), and it is of considerable interest to examine the reasons for these forms of time-variation in pressure drop.

An estimate of the component of the pressure gradient arising from inertial effects, $\mathrm{d}\hat{p}_\mathrm{I}/\mathrm{d}\hat{x}$, can be obtained by a one-dimensional, inviscid analysis, whence

$$\frac{\mathrm{d}\hat{p}_\mathrm{I}}{\mathrm{d}\hat{x}} = -\frac{\hat{\rho}}{\hat{A}}\left[\frac{\mathrm{d}\hat{Q}}{\mathrm{d}\hat{t}} + \frac{\hat{Q}^2}{\hat{A}^2}\frac{\mathrm{d}\hat{A}}{\mathrm{d}\hat{x}}\right], \tag{6}$$

where $\hat{A}(\hat{x})$ is the cross-sectional area of the tube. We can obtain an improved

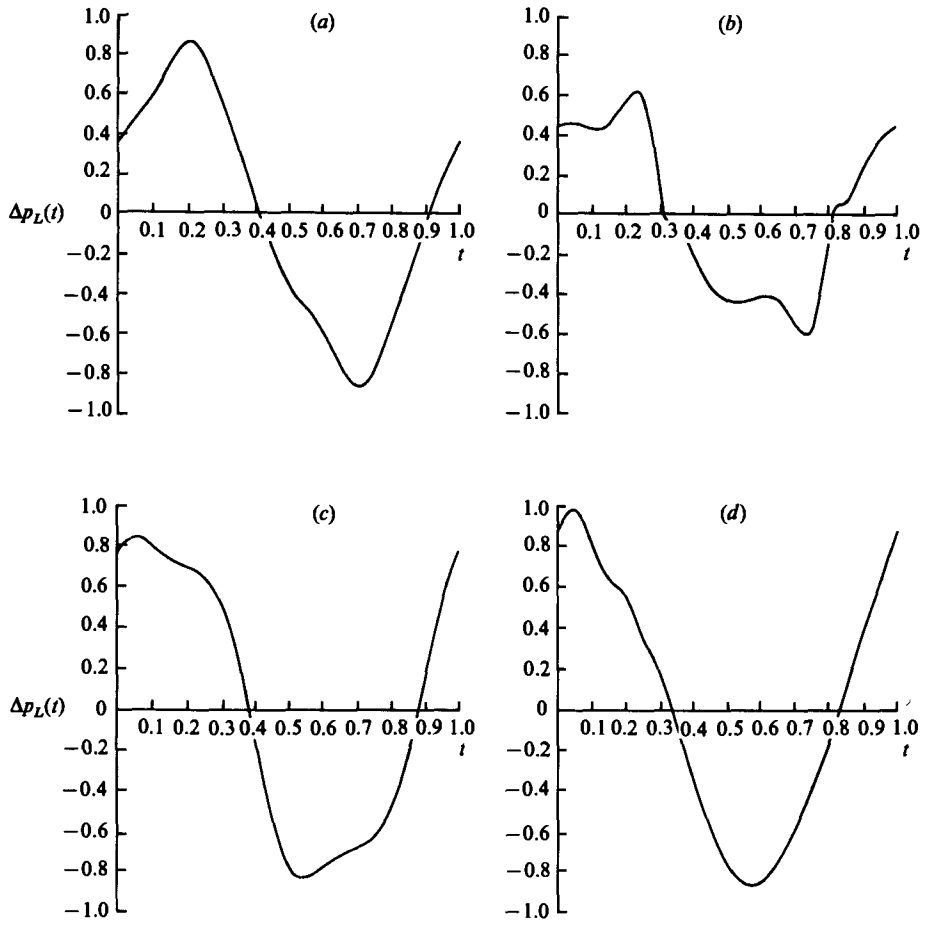

FIGURE 1. Computed variation of the dimensionless pressure drop Δp_L with time: (*a*) $Re_0 = 50$, $St = 0.01$; (*b*) $Re_0 = 200$, $St = 0.01$; (*c*) $Re_0 = 100$, $St = 0.02$; (*d*) $Re_0 = 300$, $St = 0.035$.

estimate by allowing for the 'added-mass' effect due to the non-uniformity of the walls. Thus we can define $\Delta\hat{p}_u$ by

$$\pi\hat{a}^2\Delta\hat{p}_u = \hat{a}L\hat{\rho}\frac{d\hat{Q}}{d\hat{t}} - \int_0^{\hat{a}L} \hat{p}_I\, 2\pi\hat{r}_w \frac{d\hat{r}_w}{d\hat{x}}\, d\hat{x}, \tag{7}$$

to represent approximately the pressure-drop contribution directly attributable to the unsteadiness of the flow. The first term in (7) is the result of integrating (6), and the second term, which is not affected by the datum for $\hat{p}_I$, represents the added-mass effect. If $\Delta p_u = \Delta\hat{p}_u/\hat{\rho}\hat{U}_0^2$, then using (6) and (7), and the definitions of §2, we obtain

$$\Delta p_u = 2\pi St \cos 2\pi t \left[L + 2\int_0^L g(x)\frac{dg}{dx}(x)\left[\int_0^x \frac{dx'}{g(x')^2}\right]dx\right]. \tag{8}$$

Substituting the values $L = 10$ and $D = 2$, and evaluating the integral in (8) approximately by numerical quadrature, we have

$$\Delta p_u = 24.19 St \cos 2\pi t. \tag{9}$$

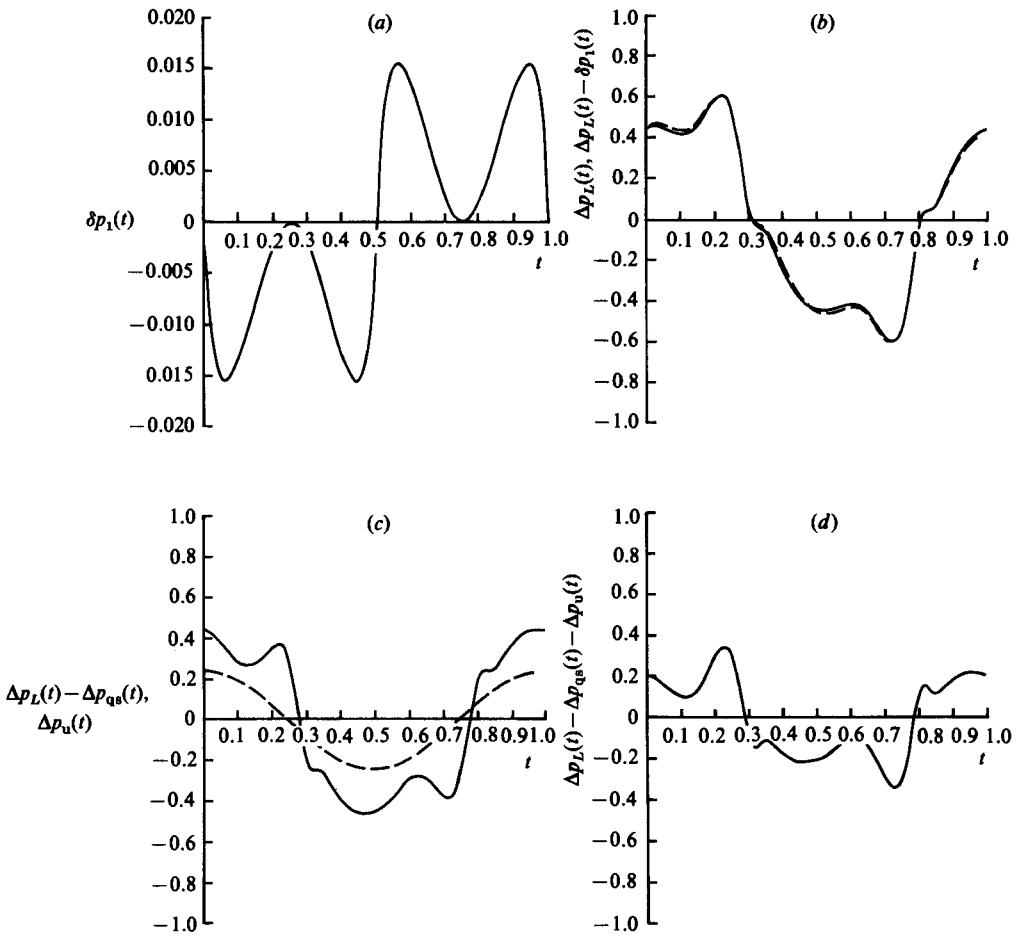

FIGURE 2. Computed variation with time of: (*a*) $\delta p_1(t)$; (*b*) $\Delta p_L(t) - \delta p_1(t)$ (dashed curve) and $\Delta p_u(t)$ (solid curve); (*c*) $\Delta p_L(t) - \Delta p_{qs}(t)$ (solid curve) and $\Delta p_u t$ (dashed curve); (*d*) $\Delta p_L(t) - \Delta p_{qs}(t) - \Delta p_u(t)$ ($Re_0 = 200$, $St = 0.01$).

Since the contribution to the pressure drop represented by Δp_u varies sinusoidally, the remaining components must account for the non-sinusoidal waveforms of figure 1. The non-sinusoidal variation may arise because the corresponding flows are distinctly non-quasi-steady (Ralph 1986) and because the steady (dimensional) pressure drop varies more rapidly than linearly with the flow rate over the range of Reynolds numbers encompassed by the flows (Ralph 1987). It remains, then, to determine the relative importance of the effects of non-quasi-steadiness and quasi-steady nonlinearity on the pressure drop.

This question has been addressed in detail for the case of figure 1(*b*). $\Delta\hat{p}_{qs} = \Delta p_{qs}\hat{\rho}\hat{U}_0^2$ is defined as the dimensional pressure drop corresponding to a steady flow at the same instantaneous flow rate (taken from Ralph 1987), and represents the pressure drop variation under the assumption of quasi-steady flow. If Δp_s now denotes the dimensionless pressure drop in a steady flow at the peak Reynolds number, then $\delta p_1(t)$, defined by

$$\delta p_1(t) = \Delta p_{qs}(t) - \Delta p_s \sin 2\pi t, \tag{10}$$

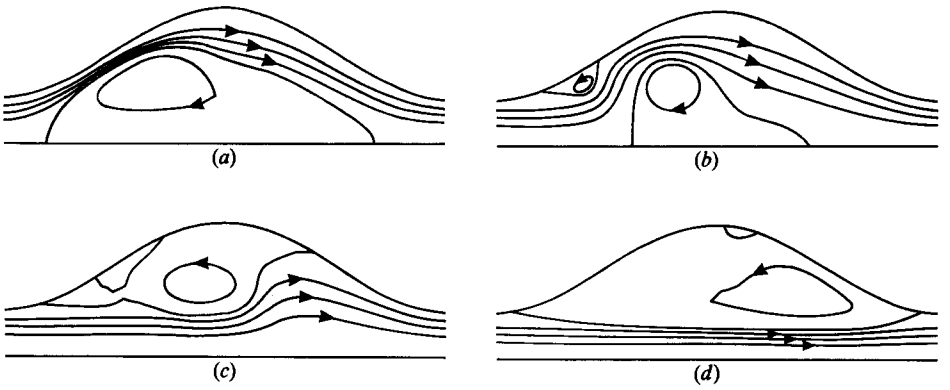

FIGURE 3. Computed instantaneous streamlines for a flow with $Re_0 = 200$, $St = 0.01$: (*a*) $t = 0.05$; (*b*) 0.15; (*c*) 0.25; (*d*) 0.45.

is a measure of the effect of quasi-steady nonlinearity on the pressure drop. A plot of $\delta p_1(t)$ is given in figure 2(*a*), and it can be seen that there are six turning points per cycle, but that the amplitude is rather small compared with the overall amplitude of Δp_L. The quantity $[\Delta p_L(t) - \delta p_1(t)]$ represents a hypothetical pressure drop from which the effect of nonlinearity has been subtracted, and is plotted in figure 2(*b*) (dashed curve). Also plotted in this figure is the actual pressure drop $\Delta p_L(t)$ (solid curve), and the close correspondence of the two curves indicates that the *direct* effect of nonlinearity is small.

Figure 2(*c*) shows $[\Delta p_L(t) - \Delta p_{qs}(t)]$ (solid curve), representing the components of pressure drop ascribable to the unsteadiness of the motion, and $\Delta p_u(t)$ (dashed curve), given by (9). The differences between these curves show that there is a considerable contribution to the pressure drop which cannot be attributed either to quasi-steady effects or, directly, to the unsteadiness of the flow. The outstanding component, $[\Delta p_L(t) - \Delta p_{qs} - \Delta p_u(t)]$, which is shown in figure 2(*d*), can only arise because the velocity field is distinctly non-quasi-steady, and we seek to explain its time-variation by considering changes in the velocity field over a half-cycle of the flow.

Flows similar to that corresponding to figures 1(*b*) and 2 are described in detail in Sobey (1980) and Ralph (1986). For ease of reference, the principal non-quasi-steady features are shown in figure 3, these being the growth of the separation region during mean-flow deceleration (figure 3*c*, *d*), and the erosion of an ejected vortex following a change in the direction of the mean flow (figure 3*a*, *b*). In addition, there are secondary separations, which would not occur quasi-steadily. Most importantly, however, the instantaneous vortex strength, as measured by the maximum value of the stream function minus its value at the wall, is much greater at times close to that of peak flow than would occur in a quasi-steady flow. For example, at $t = 0.25$ (and $t = 0.75$) the vortex strength is about five times as great as in a steady flow at the peak Reynolds number. Creation of a strong vortex is associated with significant energy production, and hence a significant pressure drop, and this leads to the pronounced turning points in figure 2(*d*) at times close to $t = 0.25$ and $t = 0.75$, when the magnitude of the pressure drop is somewhat greater than would otherwise be expected. For t between about 0.3 and 0.5 and between 0.8 and 1.0, the sign of $(\Delta p_L - \Delta p_{qs} - \Delta p_u)$ is such as to indicate a component of pressure recovery, and

during these times the vortex strength remains much greater than quasi-steady. Thus, over part of the cycle the vortex acts rather like a flywheel, storing energy as the mean flow accelerates, and returning some of this energy during the subsequent deceleration. At $t = 0.5$ and $t = 1.0$ the flow direction changes, and the persistence of the vortex near the centreline leads to greater pressure drops than would otherwise be expected. This is because the vortex acts to obstruct the main flow, forcing it into a narrow region near the wall and causing large viscous pressure drops. The turning points near $t = 0.1$ and $t = 0.6$ arise because the obstruction effect of a decaying vortex diminishes before the energy-storage effect of a new vortex becomes significant. Finally, we note the existence of a pair of turning points close to each of $t = 0.3$ and $t = 0.8$ in figure 2 (*d*), which can perhaps be related to changes in the forms of the secondary separation regions close to these times.

For figure 1 (*a*, *c*), the flow patterns show similar features to those of figure 3. Differences in the pressure-drop waveforms arise because the relative magnitudes of the components of the pressure drop differ. Thus, in figure 1 (*a*), the *direct* effect of unsteadiness is the same as in figure 1 (*b*), but the corresponding flow patterns are more nearly quasi-steady in the former case. In addition, the contribution to the pressure drop due to viscous drag is greater at all times. In figure 1 (*c*), the amplitude of the acceleration contribution is larger, and hence each overall maximum is advanced in phase.

Figure 1 (*d*) shows a rather special case, examined in detail in Ralph (1986), in which the flow is time-asymmetric: this is reflected in the pressure-drop waveform, with $\Delta p_L(t)$ at any time t not simply equal to $-\Delta p_L(t-0.5)$, as is the case for the time-symmetric flows. Note, however, that the mean value of Δp_L with respect to t remains negligible compared with its peak value: this is not a trivial result since the time-asymmetry of the flow is considerable, and the pressure drop is not directly constrained by the boundary conditions.

If the Strouhal number is increased further to values of about 0.05, the pressure-drop waveforms revert to closely sinusoidal form. This is because of both the increasing dominance of the direct effect of unsteadiness, and the decrease in the non-sinusoidal contribution due to non-quasi-steady flow patterns: this latter effect occurs because the shortened timescale of the oscillations leads to flows in which rapid variations in vortex strength do not occur. The effect of very low Strouhal numbers on pressure drop has not been investigated in detail here, but the results of Sobey (1983) and Ralph (1985) describing the relevant flow patterns indicate that the variation would be quasi-steady.

4. Variation of the pressure drop with the flow parameters

4.1. *Comparison between numerical and experimental results*

The pressure-drop waveforms obtained experimentally were affected by 'noise' to a varying degree, so that no attempt was made to compare instantaneous measured and predicted values of the pressure drop. Instead, values of $\langle|\Delta p_L|\rangle$, the time-mean of the modulus of the pressure drop, were computed from the numerical and experimental results, and these values compared for a range of Reynolds numbers and Strouhal numbers. The results are shown in figure 4.

The agreement is seen to be better at lower Strouhal numbers, with typical errors being 5% or less in figure 4 (*a*) ($St = 0.005$) but up to 20% in figure 4 (*d*) ($St = 0.02$). This is because at high Strouhal numbers the stroke lengths were relatively short and at high Reynolds numbers the viscosities relatively low, leading to small dimensional

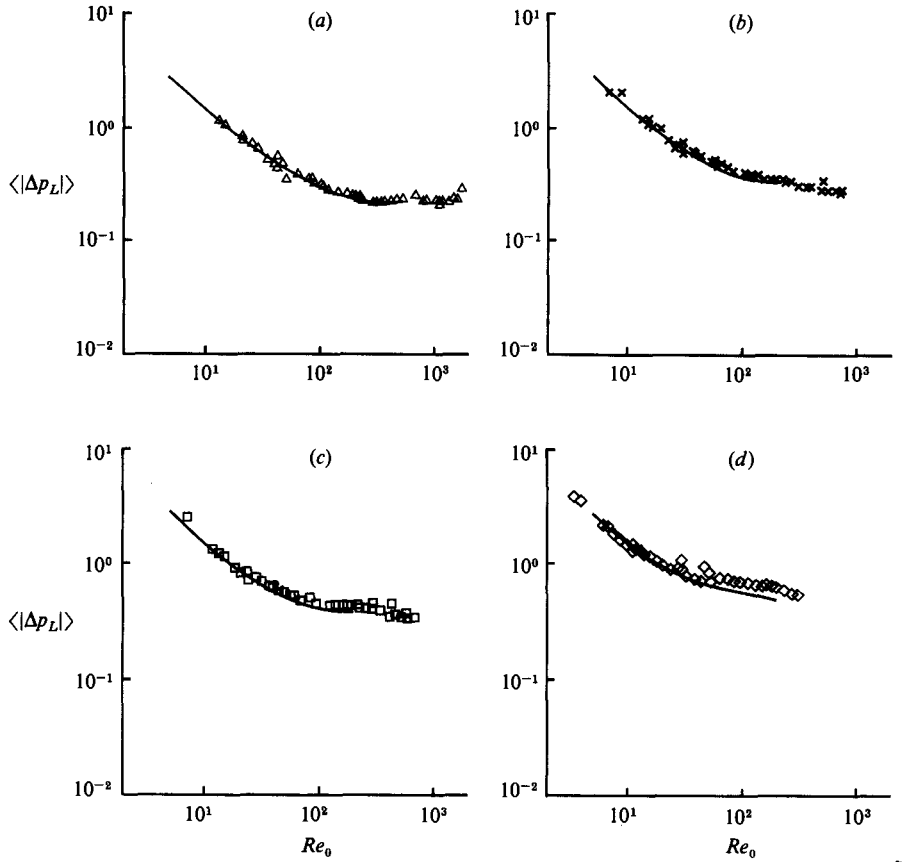

FIGURE 4. Comparison of numerical and experimental values of $\langle|\Delta p_L|\rangle$: (*a*) $St = 0.005$; (*b*) 0.008; (*c*) 0.01; (*d*) 0.02. Curves denote numerical results, geometrical symbols show experimental data.

pressure drops. A feature of the experimental pressure-drop waveforms of small dimensional amplitude was the occurrence of a large 'spike' close to each instant of flow reversal. This was due to unevenness in the running of the Scotch-yoke mechanism, which, despite considerable efforts, it proved impossible to eliminate, and which led to large accelerations and hence relatively large pressure drops. Thus, for the small-pressure-drop flows, $\langle|\Delta p_L|\rangle$ was systematically overestimated. However, calculations of the mean power dissipation in §5 show much improved agreement between experiment and prediction because the pressure 'spike', occurring as it does when the flow rate is very small, makes negligible contribution to the power dissipation. Thus the numerical results can be accepted with confidence over a greater range of flow parameters than might be suggested by figure 4.

The question of the degree of confidence that can be placed in those experimental results beyond the Reynolds-number range of the computations also requires discussion. It has been found that a 'transition-length' effect begins to affect pressure-drop measurements in steady flow; that is, the flow becomes turbulent some distance downstream of the inlet to the wavy-walled section of the tube, when the Reynolds number exceeds values of about 300 (Ralph 1987). However, since even for the lowest Strouhal numbers considered here typical fluid particles travel a maximum distance of about 2 tube wavelengths in a cycle, it is suggested that this

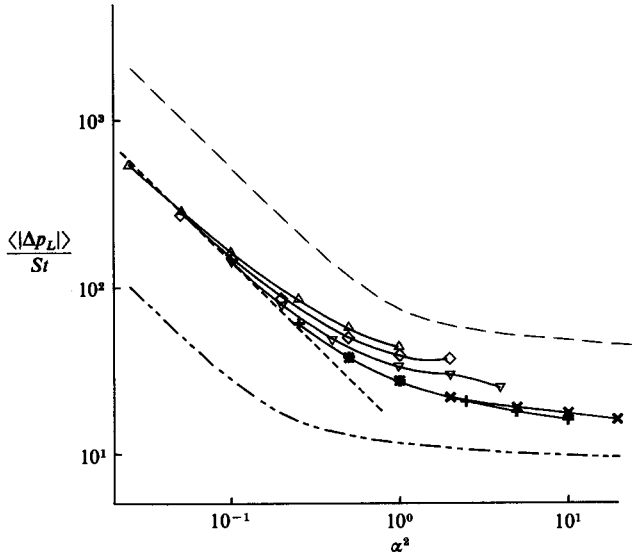

FIGURE 5. Computed variation of $\langle|\Delta p_L|\rangle/St$ with α^2 and St: $St = 0.005$ (△); 0.01 (◇); 0.02 (▽); 0.05 (+); 0.1 (×). Linear quasi-steady estimate of $\langle|\Delta p_L|\rangle$ (----). In this and remaining figures, certain dashed curves denote analytic results for straight-walled tubes: with bore equal to the minimum wavy-walled tube bore (——); with bore equal to the volume-averaged wavy walled tube bore (—·—).

transition-length effect would be less important in oscillatory flow. Furthermore, the contribution to $\langle|\Delta p_L|\rangle$ from transitional effects is small until the Reynolds number exceeds 300 throughout a significant proportion of the flow cycle. Thus, it seems unlikely that the experimental error in the measurement of $\langle|\Delta p_L|\rangle$ is greatly different when the Reynolds number is larger than the numerical limit of 200 than when it is smaller than this value.

4.2. *Further discussion of numerical results*

Standard texts on fluid mechanics give the relationship between pressure drop and flow rate for oscillatory flows in straight-walled tubes (Schlichting 1979, for example). Using the present scheme of non-dimensionalization, it can be shown that for such tubes

$$\langle|\Delta p_L|\rangle = \frac{2LSt}{|\gamma|}, \tag{11}$$

where γ is defined by

$$\gamma = \frac{1}{2} - \frac{1}{\beta}\frac{J_1(\beta)}{J_0(\beta)}, \tag{12}$$

where

$$\beta = \hat{a}\left(\frac{-\mathrm{i}2\pi\hat{f}}{\hat{\nu}}\right)^{\frac{1}{2}} = \alpha(-\mathrm{i}2\pi)^{\frac{1}{2}}. \tag{13}$$

This suggests that plotting the results for the wavy-walled tube in the form $\langle|\Delta p_L|\rangle/St$ against α^2 may collapse the data into a narrow region of the graph. Such a plot of the numerical results is given in figure 5, for Strouhal numbers in the range 0.005–0.1, and for Reynolds numbers up to 200. It can be seen that the data are

contained within a widening band of the graph as α^2 increases above about 10^{-1}, indicating that we have not obtained a single-parameter dependence: for example, when $\alpha^2 = 1$, $\langle|\Delta p_L|\rangle/St$ varies by a factor of about 2 as St varies between 0.005 and 0.1. Other plots have been examined, including $\langle|\Delta p_L|\rangle$ against α^2 and $\langle|\Delta p_L|\rangle$ and $\langle|\Delta p_L|\rangle/St$ against Re_0, but none has produced a better collapse of the data than figure 5, and we conclude that it is not possible to obtain a simple single-parameter description of the mean-modulus pressure drop (although such a description was given by Savvides & Gerrard (1984), for a restricted range of values of Reynolds number and frequency parameter). The variation of $\langle|\Delta p_L|\rangle/St$ with St at a fixed value of α^2 must be a result of the strong dependence of the non-quasi-steadiness of the flow structure on St (or equivalently Re_0) since the contribution to $\langle|\Delta p_L|\rangle$ due to unsteady inertial effects, allowing for the added-mass effect, is proportional to St and the direct effect of nonlinearity was shown in §3 to be small. However, for the range of Strouhal numbers likely to be relevant in the design of membrane mass-transfer devices, that is about 0.005–0.02, the data of figure 5 collapse into a region with about 30% variation when $\alpha^2 = 1$.

Also shown in figure 5 are the mean-modulus pressure drops in straight-walled tube flows, with (i) a straight-tube radius equal to the minimum radius of the wavy-walled tube and (ii) a straight-tube volume per unit length equal to the average volume per unit length of the wavy-walled tube. The pressure drops were made dimensionless such that the ratios of dimensional mean-modulus pressure drops would be given by ratios of the values of $\langle|\Delta p_L|\rangle/St$ on the figure (for flows with the same variation of dimensional volumetric flow rate). The straight-walled-tube values appear to bound the data for the wavy-walled tube, although the limits are widely separated. Finally, figure 5 also shows the variation of $\langle|\Delta p_L|\rangle/St$ under the assumptions of a quasi-steady, linear variation in Δp_L, with values taken from the low-Reynolds-number steady-flow results of Ralph (1987). This line appears to be an approximate asymptote for small values of α^2

5. Power dissipation and the phase relationship between pressure drop and flow rate

The dimensional instantaneous rate of pressure dissipation per wall wavelength, $\hat{P}_L(\hat{t})$, is given by

$$\hat{P}_L(\hat{t}) = \hat{Q}(\hat{t})\,\Delta p_L(\hat{t}), \tag{14}$$

and the dimensionless equivalent is $P_L(t)$:

$$P_L(t) = \frac{\hat{P}_L}{\hat{Q}_0\hat{\rho}\hat{U}_0^2} = \Delta p_L(t)\sin 2\pi t. \tag{15}$$

The time-mean value of P_L will be denoted by $\langle P_L\rangle$.

Figure 6 shows values of $\langle P_L\rangle$ obtained from the same numerical and experimental data as are represented in figure 4. The agreement is seen to be very close for all Strouhal numbers, and represents a considerable improvement, in the higher-Strouhal-number cases, over figure 4, for the reason given in §4. There is evidence of a shallow minimum in $\langle P_L\rangle$ with respect to Reynolds number at the lower Strouhal numbers and higher Reynolds numbers, and this is presumably due to the increasing turbulent energy dissipation.

With some confidence in the accuracy of the numerical scheme, we proceed to

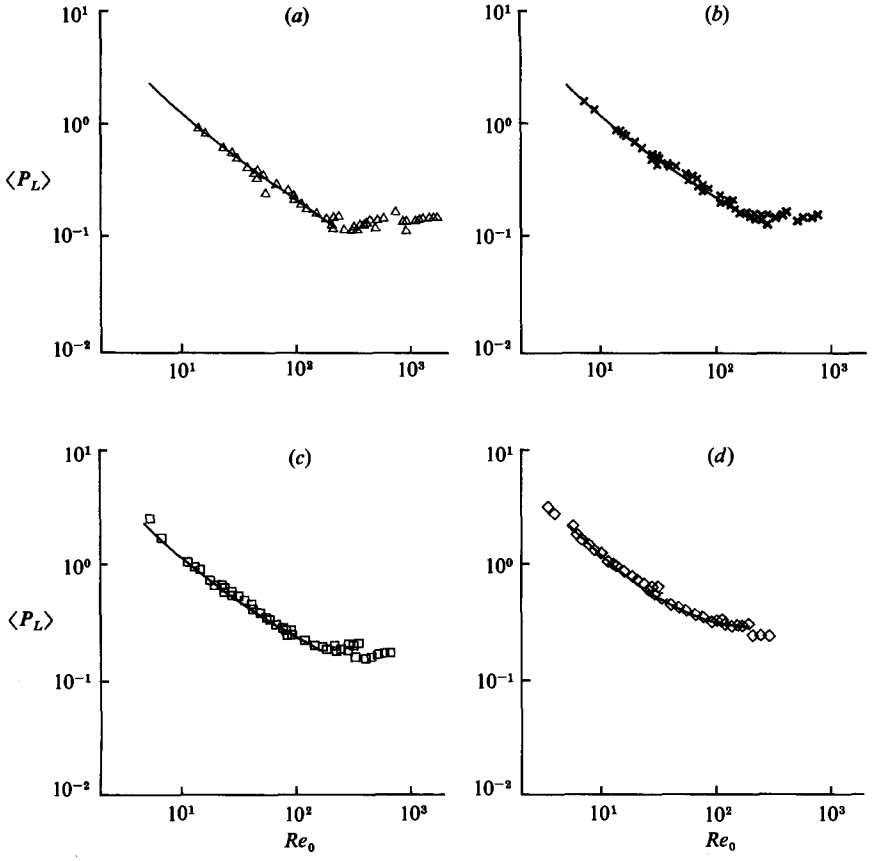

FIGURE 6. Comparison of numerical and experimental values of the mean power dissipation $\langle P_L \rangle$: (*a*) $St = 0.005$; (*b*) 0.008; (*c*) 0.01; (*d*) 0.02. Curves denote numerical results, geometrical symbols show experimental data.

consider numerically a wider range of Strouhal numbers. For a straight-walled tube, it can be shown that

$$\langle P_L \rangle = \frac{\pi L St}{2|\gamma|} \cos\theta, \tag{16}$$

where γ is defined in (12) and θ is a phase angle given by

$$\tan\theta = \frac{\mathrm{Re}\,(\gamma)}{\mathrm{Im}\,(\gamma)}. \tag{17}$$

Thus, for the wavy-walled tube, numerical values of $\langle P_L \rangle / St$ are plotted in figure 7, corresponding to the values of $\langle |\Delta p_L| \rangle$ in figure 5. Furthermore, for the straight-walled tube, (11) and (16) show that

$$\cos\theta = \frac{4}{\pi} \frac{\langle P_L \rangle}{\langle |\Delta p_L| \rangle}, \tag{18}$$

and this equation has been used to define an angle, θ, for wavy-walled tube flows where θ has a significance very similar to that of a phase angle. Numerically computed values of θ for the wavy-walled tube are shown in figure 8. (The definition of θ may break down when the flow is nearly quasi-steady and the nonlinearity of the

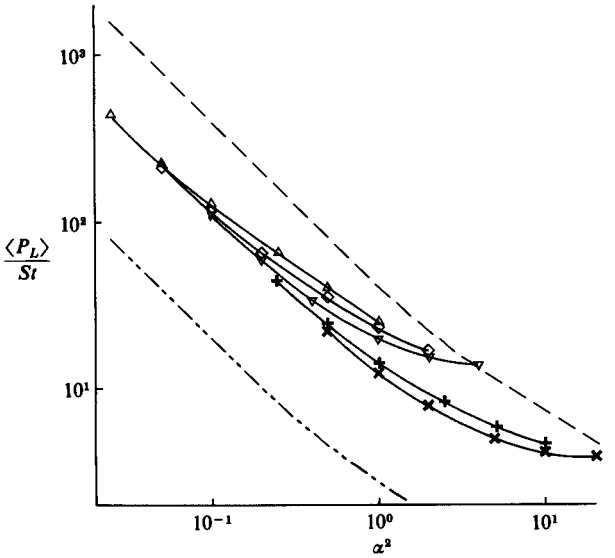

FIGURE 7. Computed variation of $\langle P_L \rangle / St$ with α^2 and St: $St = 0.005$ (△); 0.01 (◇); 0.02 (▽); 0.05 (+); 0.1 (×). For explanation of dashed curves see figure 5.

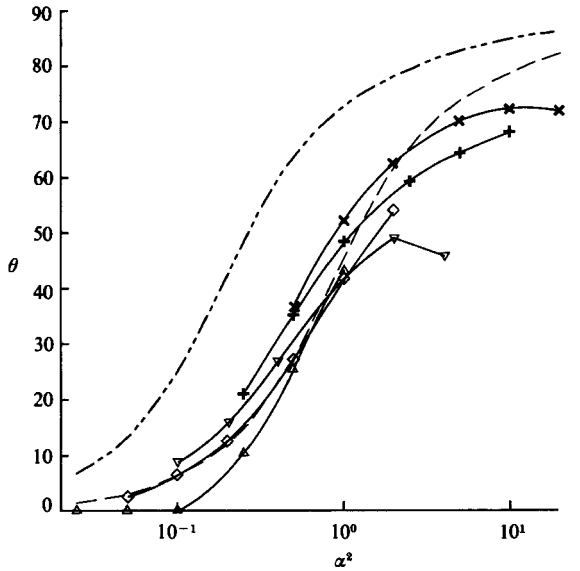

FIGURE 8. Numerical estimates of 'phase angle' θ for several values of St and α^2: $St = 0.005$ (△); 0.01 (◇); 0.02 (▽); 0.05 (+); 0.1 (×). For explanation of dashed curves see figure 5.

pressure drop – flow rate relation causes sharpening of the pressure-drop turning points. This occurred in three of the low-α^2 computations giving calculated values of $4\langle P_L \rangle / (\pi \langle |\Delta p_L| \rangle)$ greater than unity: in these cases, the phase difference was taken to be zero). Also shown on figures 7 and 8 are results for straight-walled tubes carrying flows with the same dimensional frequency and stroke volume, and with diameters equal to the minimum and volume-averaged diameters of the wavy-walled tube.

Figure 7 shows that the power dissipation is an increasingly strong function of the

Strouhal number as α^2 (or Re_0) increases, and comparison with figure 5 shows that this is more true of $\langle P_L \rangle$ than of $\langle |\Delta p_L| \rangle$. It is also true that values of $\langle P_L \rangle$ for large α^2 approach more closely (and even exceed in one case) the corresponding values for the smaller bore straight-walled tube, than to the $\langle |\Delta p_L| \rangle$ results. This is because even at quite large values of α^2 there are vortex motions and hence regions of high energy dissipation in a significant proportion of the wavy-walled-tube volume throughout most of the flow cycle. In the straight-walled tube, on the other hand, energy dissipation is confined to an increasingly thin layer at the wall as α^2 increases. It is notable that the case in which $\langle P_L \rangle$ for the wavy-walled tube exceeds that for the smaller bore straight-walled tube corresponds to the calculated flow structure with the greatest vortex strength at instants of mean-flow reversal (Ralph 1986).

The effects on the 'phase angle' θ of energy dissipation in vortices are seen to be marked. Thus, figure 8 shows that the phase angle often corresponds to that in a straight-walled tube whose bore is smaller than the minimum bore of the wavy-walled tube. The highest-Strouhal-number case does not appear to be approaching a limit of 90°, suggesting that at this Strouhal number, increasing α^2 (and hence Re_0) would lead to flows in which vortical dissipation remained important. An unexpected feature of figure 8 is that for a Strouhal number of 0.02, increasing α^2 from 2 to 4 results in a *decrease* in θ: this change in α^2 corresponds to a dramatic increase in both the vortex strength and the time for which an ejected vortex persists at the centreline. Thus, there are significant increases in the pressure-drop contributions owing to both the blockage and energy-storage effects of non-quasi-steady vortices, and since these contributions are 'in phase' with the flow, there is a reduction in the phase angle.

6. Discussion and conclusions

It has been shown that in oscillatory wavy-walled-tube flows, in which the flow rate varies sinusoidally with time, the pressure-drop variation may be distinctly non-sinusoidal. This effect is most marked when the mean-flow acceleration contribution to the pressure drop is not dominant but the flow field is, nevertheless, non-quasi-steady.

Simplified models of stenosis flows have been based on the assumption that the pressure drop can be represented as the sum of a quasi-steady part and a contribution to produce accelerations of the mean flow (Young & Tsai 1973 and Newman, Westerhof & Sipkema 1979). These models assume that the dimensionless peak pressure drop is given by a term dependent solely on the stenosis geometry, plus a term increasing with decreasing Reynolds number but independent of the frequency parameter. The inadequacy of these assumptions for wavy-walled-tube flows in the parameter regimes investigated in the current paper has already been demonstrated (§4). The point is further illustrated in figure 9, in which are plotted values of the ratios

$$R_1 = \frac{\langle |\Delta p_L| \rangle}{\langle |\Delta p_{\rm qs} + \Delta p_{\rm u}| \rangle} \tag{19}$$

and

$$R_2 = \frac{\max(\Delta p_L)}{\max(\Delta p_{\rm qs} + \Delta p_{\rm u})} \tag{20}$$

(where the maxima are taken with respect to time), for several values of α^2 and Re_0. As Re_0 increases, it can be seen that R_1 and R_2 tend to increase, and that a maximum with respect to α^2 develops, with a turning point where α^2 is of order unity.

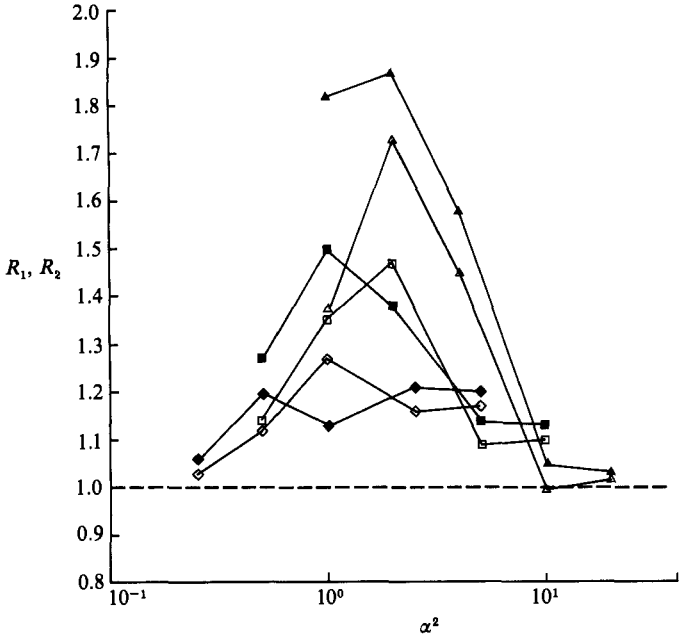

FIGURE 9. Computed variation of R_1 (unfilled symbols) and R_2 (filled symbols) with α^2 for three Reynolds numbers: $Re_0 = 50$ (◇, ◆); 100 (□, ■); 200 (△, ▲).

Thus there is strong dependence of the pressure drop on the frequency parameter, and it is also clear that the assumptions of the simple stenosis models would lead to the peak pressure drop being underestimated by almost 50% in some cases.

It can be concluded, then, that for unsteady separating flows in which the nonlinear, inertial and unsteady terms of the Navier–Stokes equations are all important, the pressure drop can only be predicted with reasonable accuracy by allowing for the *interaction* of these terms in generating non-quasi-steady fluid motions.

I should like to express my sincere thanks to Dr I. J. Sobey of Schlumberger Research, Cambridge for his invaluable assistance in this work and to Dr T. J. Pedley of D.A.M.T.P., Cambridge University for many useful suggestions. I wish also to thank members of the Medical Engineering Unit of Oxford University, where this work was carried out, including Drs J. W. Stairmand and B. J. Bellhouse for useful advice and M. A. L. Stevenson, G. Walker and J. Greenford for technical assistance. I acknowledge receipt of a Science and Engineering Research Council postgraduate studentship.

REFERENCES

BELLHOUSE, B. J., BELLHOUSE, F. H., CURL, C. M., MACMILLAN, T. I., GUNNING, A. J., SPRATT, E. H., MACMURRAY, S. B. & NELEMS, J. M. 1973 A high efficiency membrane oxygenator and pulsatile pump and its application to animal trials. *Trans. Am. Soc. Artif. Int. Organs* **19**, 72–79.

BELLHOUSE, B. J. & SNUGGS, R. A. 1977 Augmented mass transfer in a membrane lung and a hemo-dialyser using vortex mixing. *INSERM-Euromech 92* **71**, 371–384.

CHANG, H. K. & MOCKROS, L. F. 1971 Blood-gas transfer in an axial flow annular oxygenator. *AIChE J.* **17**, 397–401.

CHENG, L. C., CLARK, M. E. & ROBERTSON, J. M. 1972 Numerical calculations of oscillating flow in the vicinity of square wall obstacles in plane conduits. *J. Biomech.* **5**, 467–484.

CHENG, L. C., ROBERTSON, J. M. & CLARK, M. E. 1973 Numerical calculations of oscillatory non-uniform flow. II. Parametric study of pressure gradient and frequency with square wall obstacles. *J. Biomech.* **6**, 521–538.

CLARK, C. 1976*a* The fluid mechanics of aortic stenosis. I. Theory and steady flow experiments. *J. Biomech.* **9**, 521–528.

CLARK, C. 1976*b* The fluid mechanics of aortic stenosis. II. Unsteady flow experiments. *J. Biomech.* **9**, 567–573.

DALY, B. J. 1976 A numerical study of pulsatile flow through stenosed canine femoral arteries. *J. Biomech.* **9**, 465–475.

GHADDAR, N. K., KORCZAK, K. Z., MIKIC, B. B. & PATERA, A. A. 1986 Numerical investigation of incompressible flow in grooved channels. Part I. Stability and self-sustained oscillations. *J. Fluid Mech.* **163**, 99–127.

NEWMAN, D. L., WESTERHOF, N. & SIPKEMA, P. 1979 Modelling of aortic stenosis. *J. Biomech.* **12**, 229–235.

RALPH, M. E. 1985 Flows in wavy-walled tubes. D.Phil. thesis, University of Oxford.

RALPH, M. E. 1986 Oscillatory flows in wavy-walled tubes. *J. Fluid Mech.* **168**, 515–540.

RALPH, M. E. 1987 Steady flow structures and pressure drops in wavy-walled tubes. *Trans. ASME I: J. Fluids Engng.*

SAVVIDES, G. N. & GERRARD, J. H. 1984 Numerical analysis of the flow through a corrugated tube with application to arterial prosthesis. *J. Fluid Mech.* **138**, 129–160.

SCHLICHTING, H. 1979 *Boundary-Layer Theory*, 7th edn. McGraw-Hill.

SOBEY, I. J. 1980 On flow through furrowed channels. Part I. Calculated flow patterns. *J. Fluid Mech.* **96**, 1–26.

SOBEY, I. J. 1983 The occurrence of separation in oscillatory flow. *J. Fluid Mech.* **134**, 247–257.

STEPHANOFF, K. D., SOBEY, I. J. & BELLHOUSE, B. J. 1980 On flow through furrowed channels. Part 2. Observed flow patterns. *J. Fluid Mech.* **99**, 27–32.

YOUNG, D. F. & TSAI, F. Y. 1973 Flow characteristics in models of arterial stenoses – II. Unsteady flow. *J. Biomech.* **6**, 547–559.